Finite element based N-Port model for preliminary design of multibody systems

Francesco Sanfedino [a,*], Daniel Alazard [a], Valérie Pommier-Budinger [a], Alexandre Falcoz [b], Fabrice Boquet [c]

[a] Institut Supérieur de l'Aéronautique et de l'Espace (ISAE-SUPAERO), Université de Toulouse, 10 Avenue Edouard Belin, BP-54032, 31055, Toulouse Cedex 4, France
[b] Airbus Defence and Space, 31 Rue des Cosmonautes Z.I. du Palays, 31402, Toulouse Cedex, France
[c] ESA/ESTEC, Keplerlaan 1, 2201 AZ, Noordwijk, The Netherlands

A B S T R A C T

This article presents and validates a general framework to build a linear dynamic Finite Element-based model of large flexible structures for integrated Control/Structure design. An extension of the Two-Input Two-Output Port (TITOP) approach is here developed. The authors had already proposed such framework for simple beam-like structures: each beam was considered as a TITOP sub-system that could be interconnected to another beam thanks to the ports. The present work studies bodies with multiple attaching points by allowing complex interconnections among several sub-structures in tree-like assembly. The TITOP approach is extended to generate NINOP (N-Input N-Output Port) models. A Matlab toolbox is developed integrating beam and bending plate elements. In particular a NINOP formulation of bending plates is proposed to solve analytic two-dimensional problems. The computation of NINOP models using the outputs of a MSC/Nastran modal analysis is also investigated in order to directly use the results provided by a commercial finite element software. The main advantage of this tool is to provide a model of a multibody system under the form of a block diagram with a minimal number of states. This model is easy to operate for preliminary design and control. An illustrative example highlights the potential of the proposed approach: the synthesis of the dynamical model of a spacecraft with two deployable and flexible solar arrays.

Keywords:
Multibody dynamics
Mechanical preliminary design
Bending plate
Model reduction

1. Introduction

Structural and control co-design has attracted a particular interest in the last three decades thanks to the efforts which have been made to combine the different requirements of the two disciplines. In particular in Space applications the development of larger and more flexible satellite structures makes flexible mode analysis mandatory [1]. Large appendages correspond to low flexible modes that have to be taken into account to design and optimize appropriate control laws.

However the analysis of large structures involves complex model synthesis based on a large amount of degrees-of-freedom (DOFs) with high computational costs and difficult structural understanding. As a consequence the efforts of researchers have focused on exploration of substructuring techniques consisting in analyzing large complex structures separately by a multibody approach. This approach makes it possible to deal with simpler models subjected to different constraint conditions and mechan-

* Corresponding author.
E-mail addresses: francesco.sanfedino@isae.fr (F. Sanfedino), daniel.alazard@isae.fr (D. Alazard), valerie.budinger@isae.fr (V. Pommier-Budinger), alexandre.falcoz@airbus.com (A. Falcoz), Fabrice.Boquet@esa.int (F. Boquet).

https://doi.org/10.1016/j.jsv.2017.11.021

ical properties and facing the control issue at the same time. Examples of applications are the verification of spacecraft stability robustness as in Ref. [2] or the analysis of collocated actuators as in Ref. [3].

Moreover, all the methods developed in the multibody context can benefit from the powerful results provided by the Finite Element Method (FEM), the most widely used and proven numerical method in structural analysis.

Two methods which include FEM results in a substructure approach are widespread: the Finite Element-Transfer Matrix (FE-TM) method and the component modes synthesis (CMS). The Transfer Matrix method was first introduced by Holzer in 1921 [4] and independently by Myklestad in 1945 [5]. Recently, it was somewhat revived by Rui et al. [6], with specific reference to the multibody dynamic field. The FE-TM combines the finite element approach with transfer matrix models, whose basis were already stated by Leckie and Pestel [7]. The basic principle is the connection of flexible structures in series by simple multiplication of their transfer functions, characterized by the relation between the state vector computed at the left and right points of the single body. Each state vector is defined by two contributions: the generalized displacements of the point and the corresponding generalized forces. Its application to FEM procedure in vibration analysis allowed Dokainish [8] to considerably reduce model complexity (stiffness and mass matrix size) and computational cost without any reduction of DOF. The FE-TM approach was then applied for chain-like structure analysis [9] and closed-loop kinematic chain of flexible structures like the four-bar mechanism [10]. A modified version of FE-TM allowed researchers to extend the method to Space structures for control purposes: Tan et al. [11] proposed the collocated control of a beam by Linear Quadratic Regulator (LQR) theory. Rui et al. [12] provided the dynamic model of a multiple launch rocket system. Modern application of Transfer Matrix method can be found in Ref. [13] for the real-time control of multibody systems and in Ref. [14] to analyze complex mufflers.

There are mainly two limitations in FE-TM formulation: the first one comes from the derivation of the transfer-matrix which requires the inversion of the sub-matrices associated with each element [11], that is possible if and only if these sub-matrices are non-singular and square; the second one consists in the difficulty to model non tree-like multibody structures with both multiple input and multi output ends [15]. The latter limitation is an important issue in the Space field, where complex and different flexible appendages such as solar arrays, antennas or robotic arms are attached to the spacecraft's central body. For this type of application the information for control and design purposes is the dynamic model at the tree attachment point.

The CMS approach [16–18] has earned a great following in the aerospace sector thanks to its matrix condensation reduction well suited for substructuring problems [19–22]. Young [3] proposed the so called controlled component synthesis (CCS) based on the CMS theory for large flexible structures like planar trusses. He demonstrated the integration of the structure modeling and the decentralized control design at the component level of a complex body divided into a collection of substructures. The limitations of this approach come from the overlapping of the different components done at the matrix level. In-depth knowledge of the FEM models was thus mandatory.

Later many methods based on the effective mass/inertia model of each flexible appendage of a complex structure [23] or on the impedance matrix [24] were developed. All these methods inherited from Craig, Bampton and Chang's works [25,26] as particular cases of CMS approach. Regarding the mass/inertia approach, many important contributions [1,2,27] have to be cited. They all proposed a way to obtain a linear dynamic model of a spacecraft with different appendages for an Attitude and Orbital Control System (AOCS). In particular they took into account the influence of each flexible appendage on the spacecraft rigid hub. The main drawback of these models is the loss of the dynamic information corresponding to the free tip appendage points. As a consequence the representation of multiple flexible body in chain-like configuration was not technically possible. The Two-Input Two-Output (TITOP) Port model, proposed for the first time by Alazard et al. [28], finally overcame this limitation. It conceives the dynamic model of each substructure as a transfer between the accelerations and the external forces at each connection point in a state-space form. It embeds, in the same minimal state-space representation, the direct and inverse dynamic models of the substructure for any kind of complex boundary conditions. One of the greatest advantages of the TITOP model is the invertibility of all sub-element channels: any kind of boundary conditions can be solved starting from the same model. Murali et al. [29] proposed an analytical model of a uniform beam in TITOP approach to model a spacecraft sub-structured antenna. Perez et al. [30,31] stated the basis for the model parametrization in Linear Fractional Representation (LFT) form for co-design/robust control of TITOP assemblies. Perez et al. [32] finally presented a rigorous formalization of the TITOP approach with a comparison with non-linear existing models.

Chebbi [33] completed the formulation by presenting a rigorous comparison of the TITOP model of a uniform beam, the same stated in Ref. [29], for several boundary conditions, with results provided by the Euler-Bernoulli theory. In particular, in this work, the problem of model inversion was directly addressed for the first time by application. Thanks to the latter, a closed-loop four-bar mechanism was analyzed.

However all the previous works only dealt with simple beams in direct chainlike assembly.

The main contribution of the present work is to better investigate the TITOP inversion operation in order to provide coherent models not only for analytical simple models but also for numerical models provided by FEM commercial software products. This need is essential in order to use the TITOP approach in the case of structures modeled by FEM with complex boundary conditions. Moreover the TITOP approach will be extended to two-dimensional problems to build N-Input N-Output Port models (NINOP). The case of a bending plate will be treated analytically with the NINOP approach and an application to a deployable spacecraft solar array will be provided. In this case the NINOP model will provide the dynamic information of multiple free points of the flexible substructure. This work aims at providing preliminary design tools and a framework for the Control/Structure design of large flexible appendages by taking into account the needs of both disciplines: a true description of the structural flexibility and a minimal representation of the system's dynamic behaviour (no excessive number of states) for control purposes. To achieve this objective, the TITOP/NINOP approach is proposed and developed in Sec. 2. The analysis of the channel inversion is addressed

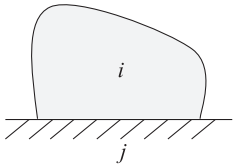

Fig. 1. Internal (i) and junction (j) DOFs of a structure.

in Sec. 3 applied to a clamped-free beam problem. The NINOP approach is applied to a bending plate in Sec. 4 and an application to a satellite deployable solar array is shown in Sec. 4.2. Finally Sec. 5 outlines the main contributions of the present work.

2. TITOP and NINOP models

2.1. Formalism of the dynamic analysis

The TITOP method introduced in Ref. [28] is based on the Craig-Bampton method [34] (particular case of CMS method) where the dynamic analysis is performed by a modal approach. The formalization used in this paper is based on Girard and Roy's synthesis [23]. The basis of the modal approach consists in two steps:

1. The resolution of the motion equation without any excitation source, which provides the so called 'normal modes';
2. The superposition of the modes.

Let us consider a general structure (Fig. 1). In its complete set of DOFs two sets can be distinguished: the internal DOFs (subscript i) and the junction DOFs (subscript j). By definition, the excitation is an external force/torque and the response is a motion (linear or angular displacement, speed or acceleration) for the internal DOFs. Conversely if the excitation is a motion, the response is a force/torque (in particular the reaction forces/torques will be considered) for the junction DOFs.

The classical second order equation of motion of the structure obtained by Lagrangian formulation using the FEM method can be written thanks to matrix representation as:

$$\begin{bmatrix} \mathbf{M}_{ii} & \mathbf{M}_{ij} \\ \mathbf{M}_{ji} & \mathbf{M}_{jj} \end{bmatrix} \begin{bmatrix} \ddot{\mathbf{u}}_i \\ \ddot{\mathbf{u}}_j \end{bmatrix} + \begin{bmatrix} \mathbf{C}_{ii} & \mathbf{C}_{ij} \\ \mathbf{C}_{ji} & \mathbf{C}_{jj} \end{bmatrix} \begin{bmatrix} \dot{\mathbf{u}}_i \\ \dot{\mathbf{u}}_j \end{bmatrix} + \begin{bmatrix} \mathbf{K}_{ii} & \mathbf{K}_{ij} \\ \mathbf{K}_{ji} & \mathbf{K}_{jj} \end{bmatrix} \begin{bmatrix} \mathbf{u}_i \\ \mathbf{u}_j \end{bmatrix} = \begin{bmatrix} \mathbf{F}_i \\ \mathbf{F}_j \end{bmatrix} \tag{1}$$

where $\mathbf{u}$, $\dot{\mathbf{u}}$ and $\ddot{\mathbf{u}}$ are respectively the linear/angular displacement, speed and acceleration of the complete set of DOFs taken into account. They are associated with each node of a FEM discretization of the considered structure. The symmetric matrices $\mathbf{M}$, $\mathbf{C}$ and $\mathbf{K}$ are respectively the mass, damping and stiffness matrices obtained by the FEM synthesis. Finally $\mathbf{F}_i$ are the forces/torques imposed on the internal DOFs and $\mathbf{F}_j$ are the reaction forces/torques imposed on the structure by the junction. Note that for the generic symmetric matrix $\mathbf{X}$ ($\mathbf{M}$, $\mathbf{C}$ or $\mathbf{K}$), $\mathbf{X}_{ij}^{\mathrm{T}} = \mathbf{X}_{ji}$.

The normal modes are obtained from the solution of the equation of motion without any excitation ($\mathbf{F}_i = \mathbf{0}_i$, $\mathbf{u}_j = \mathbf{0}_j$). Two equations are obtained from Eq. (1). Let us concentrate on the first one which allows us to solve $\mathbf{u}_i$. If the damping term is neglected this homogeneous equation takes the form:

$$\mathbf{M}_{ii}\ddot{\mathbf{u}}_i + \mathbf{K}_{ii}\mathbf{u}_i = \mathbf{0}_i \tag{2}$$

The solution of this problem corresponds to the well known eigenvalues/eigenvectors system of N equations (where N is the total number of internal DOFs):

$$(-\omega_k^2\mathbf{M}_{ii} + \mathbf{K}_{ii})\mathbf{\Phi}_{ik} = \mathbf{0}_i \tag{3}$$

with $k = 1 \ldots N$ and ω_k and $\mathbf{\Phi}_{ik}$ are respectively the k-eigenvalue and the associated k-eigenvector.

After resolution of Eq. (2) the complete Eq. (1) is solved by projection of all the physical proprieties onto the base composed by the already computed modes $\mathbf{\Phi}_{ik}$ and the so called *junction modes* matrix $\mathbf{\Psi}$ obtained by successively imposing a unit displacement $\mathbf{u}_j$, while blocking all other junction displacements ($\dot{\mathbf{u}}_j = 0$, $\ddot{\mathbf{u}}_j = 0$). For cases with a single junction the junction modes verify [23]:

$$\mathbf{\Psi}_{jj} = \mathbf{I}_{jj} \tag{4}$$

where $\mathbf{I}$ is the identity matrix and

$$\mathbf{K}_{ii}\mathbf{\Psi}_{ij} + \mathbf{K}_{ij} = \mathbf{0}_{ij} \Rightarrow \mathbf{\Psi}_{ij} = -\mathbf{K}_{ii}^{-1}\mathbf{K}_{ij} \tag{5}$$

The projection onto the base composed by the normal and junction modes allows us to perform the Craig-Bampton transformation $\mathbf{\Omega}_{i+j,k+j}$ [34]:

$$\begin{bmatrix}\mathbf{u}_i\\ \mathbf{u}_j\end{bmatrix} = \begin{bmatrix}\mathbf{\Phi}_{ik} & \mathbf{\Psi}_{ij}\\ \mathbf{0}_{jk} & \mathbf{I}_{jj}\end{bmatrix}\begin{bmatrix}\boldsymbol{\eta}_k\\ \mathbf{u}_j\end{bmatrix} = \mathbf{\Omega}_{i+j,k+j}\begin{bmatrix}\boldsymbol{\eta}_k\\ \mathbf{u}_j\end{bmatrix} \tag{6}$$

where $\boldsymbol{\eta}_k$ are the modal displacements. $\mathbf{\Omega}_{i+j,k+j}$, introduced in Eq. (1), gives the new form of the equation of motion:

$$\begin{bmatrix}\mathbf{m}_{kk} & \mathbf{L}_{kj}\\ \mathbf{L}_{jk} & \overline{\mathbf{M}}_{jj}\end{bmatrix}\begin{bmatrix}\ddot{\boldsymbol{\eta}}_k\\ \ddot{\mathbf{u}}_j\end{bmatrix} + \begin{bmatrix}\mathbf{c}_{kk} & \mathbf{0}_{kj}\\ \mathbf{0}_{jk} & \mathbf{0}_{jj}\end{bmatrix}\begin{bmatrix}\dot{\boldsymbol{\eta}}_k\\ \dot{\mathbf{u}}_j\end{bmatrix} + \begin{bmatrix}\mathbf{k}_{kk} & \mathbf{0}_{kj}\\ \mathbf{0}_{jk} & \overline{\mathbf{K}}_{jj}\end{bmatrix}\begin{bmatrix}\boldsymbol{\eta}_k\\ \mathbf{u}_j\end{bmatrix} = \begin{bmatrix}\mathbf{\Phi}_{ki}\mathbf{F}_i\\ \mathbf{\Psi}_{ji}\mathbf{F}_i + \mathbf{F}_j\end{bmatrix} \tag{7}$$

where:

- $\mathbf{m}_{kk} = \mathbf{\Phi}_{ki}\mathbf{M}_{ii}\mathbf{\Phi}_{ik}$ is the diagonal matrix of the generalized masses m_k. The eigenvectors in $\mathbf{\Phi}_{ik}$ can be normalized in such a way that $\mathbf{m}_{kk} = \mathbf{I}_{kk}$.
- $\mathbf{c}_{kk} = \mathbf{\Phi}_{ki}\mathbf{C}_{ii}\mathbf{\Phi}_{ik}$ is the damping matrix. It is assumed diagonal, i.e. $\mathbf{c}_{kk} = \mathrm{diag}(2\zeta_k\omega_k m_k)$, after neglecting the intermodal damping terms, although such condition is only strictly met when the damping matrix is proportional to the mass and stiffness matrices;
- $\mathbf{k}_{kk} = \mathbf{\Phi}_{ki}\mathbf{K}_{ii}\mathbf{\Phi}_{ik} = \mathrm{diag}(m_k\omega_k^2)$ is the diagonal matrix of the generalized stiffnesses k_k;
- $\mathbf{L}_{kj} = \mathbf{\Phi}_{ki}(\mathbf{M}_{ii}\mathbf{\Psi}_{ij} + \mathbf{M}_{ij})$ is the matrix of the participation factors;
- $\overline{\mathbf{M}}_{jj} = \mathbf{\Psi}_{ji}\mathbf{M}_{ii}\mathbf{\Psi}_{ij} + \mathbf{\Psi}_{ji}\mathbf{M}_{ij} + \mathbf{M}_{ji}\mathbf{\Psi}_{ij} + \mathbf{M}_{jj}$ is the condensed mass matrix. In case of a rigid statically determinate junction (junction represented by one and only one node) this matrix is exactly equal to the rigid body matrix $\mathbf{M}_{\mathrm{rr}}$ of the considered structure. This one includes the information about the mass, the inertia and the center of mass of the structure with respect to the unique junction node;
- $\overline{\mathbf{K}}_{jj} = \mathbf{K}_{jj} - \mathbf{K}_{ji}\mathbf{K}_{ii}^{-1}\mathbf{K}_{ij}$ is the condensed stiffness matrix, equal to $\mathbf{0}_{jj}$ in case of a rigid statically determinate junction.

In TITOP approach [28,29] a previous coordinate transformation before starting the modal analysis by Eq. (3) allows us to have a largely simplified equivalent version of the problem in Eq. (7) and $\mathbf{m}_{kk} = \mathbf{I}_{kk}$ without any normalization operation. This fact will be more extensively addressed in Section 2.2.

2.2. The TITOP approach

Let us consider the i-th flexible linking appendage $\mathcal{L}_i$ taking part in a complex sub-structured body (Fig. 2). It is discretized by a FEM approach and is linked to the parent sub-structure $\mathcal{L}_{i-1}$ by the node P and to the child sub-structure $\mathcal{L}_{i+1}$ by the node C. In the TITOP model, the node P is considered as a rigid or statically determinate junction (called thereafter junction node and characterized by clamped boundary condition) and the node C is considered as an internal node and is characterized by free boundary condition. This first assumption does not constrain the dynamic analysis to the *clamped-free* condition as already demonstrated in Ref. [33] for an homogeneous beam, but it allows simplifying Eq. (7) without any loss of information and studying any kind of boundary conditions.

Let us consider that the mesh of $\mathcal{L}_i$ globally contains N_n nodes and, in the general case, each node has 6 DOFs (3 translations and 3 rotations). The vectors $\mathbf{u}$, $\dot{\mathbf{u}}$, $\ddot{\mathbf{u}}$ and $\mathbf{F}$ in Eq. (1) will have globally $N_g = 6N_n$ components and FEM matrices will be $N_g \times N_g$ matrices. Moreover let us define $N = N_g - 6$ the total number of the internal DOFs and the inertial frame $\mathcal{R}_0 = (P^0, \mathbf{x}_0, \mathbf{y}_0, \mathbf{z}_0)$

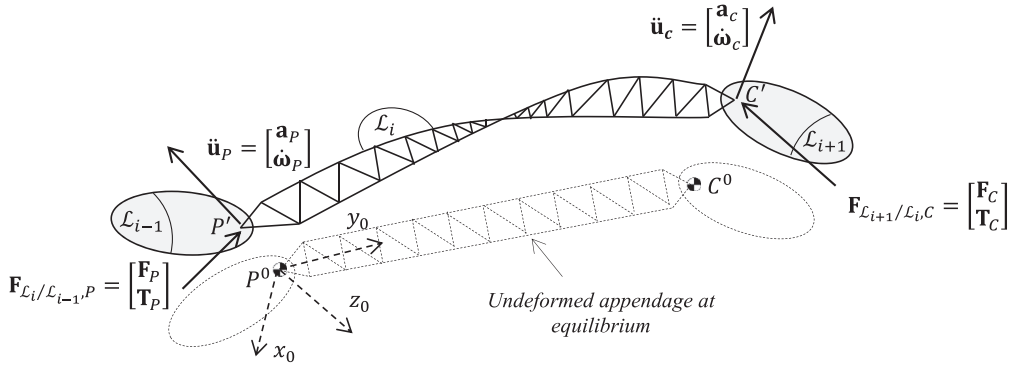

Fig. 2. i-th flexible appendage of a complex sub-structured body.

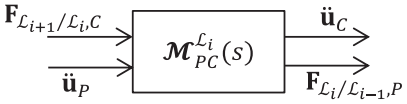

Fig. 3. TITOP model $\mathcal{M}_{PC}^{\mathcal{L}_i}(s)$ block-diagram.

centered in node P of $\mathcal{L}_i$ in equilibrium condition.

The TITOP model $\mathcal{M}_{PC}^{\mathcal{L}_i}(s)$ (where s is the Laplace variable) is a linear state-space model with 12 inputs (6 for each of the two input ports):

1. The 6 components in $\mathcal{R}_0$ of the wrench $\mathbf{F}_{\mathcal{L}_{i+1}/\mathcal{L}_i,C}$ composed of the three-components force vector $\mathbf{F}_C$ and the three-components torque vector $\mathbf{T}_C$ applied by $\mathcal{L}_{i+1}$ to $\mathcal{L}_i$ at the free node C;
2. The 6 components in $\mathcal{R}_0$ of the acceleration vector $\ddot{\mathbf{u}}_P$ composed of the three-components linear acceleration vector $\mathbf{a}_P$ and the three-components angular acceleration vector $\dot{\boldsymbol{\omega}}_P$ at the clamped node P;

and 12 outputs (6 for each of the two output ports):

1. The 6 components in $\mathcal{R}_0$ of the acceleration vector $\ddot{\mathbf{u}}_C$ at the free node C;
2. The 6 components in $\mathcal{R}_0$ of the wrench $\mathbf{F}_{\mathcal{L}_i/\mathcal{L}_{i-1},P}$ applied by $\mathcal{L}_i$ to the parent structure $\mathcal{L}_{i-1}$ at the clamped node P.

In Fig. 3 a block diagram of the TITOP model $\mathcal{M}_{PC}^{\mathcal{L}_i}(s)$ is illustrated.

The matrix $\mathcal{M}_{PC}^{\mathcal{L}_i}(s)$ is constructed using the terms of Eq. (1) computed by a FEM analysis. In this case P is a junction node, so the subscript substitution $j = P$ is admitted. Besides we get $\mathbf{F}_j = -\mathbf{F}_{\mathcal{L}_i/\mathcal{L}_{i-1},P}$ and $\mathbf{F}_i = \mathbf{F}_{\mathcal{L}_{i+1}/\mathcal{L}_i,C}$. Now a coordinate transformation $\boldsymbol{\Omega}_P$ is performed in order to have all the internal DOFs i with respect to the reference frame $\mathcal{R}_0$:

$$\begin{bmatrix}\mathbf{u}_i\\ \mathbf{u}_P\end{bmatrix} = \begin{bmatrix}\mathbf{I}_{ii} & \boldsymbol{\tau}_{CP}\\ \mathbf{0}_{Pi} & \mathbf{I}_{66}\end{bmatrix}\begin{bmatrix}\widetilde{\mathbf{u}}_i\\ \mathbf{u}_P\end{bmatrix} = \boldsymbol{\Omega}_P\begin{bmatrix}\widetilde{\mathbf{u}}_i\\ \mathbf{u}_P\end{bmatrix} \tag{8}$$

where $\boldsymbol{\tau}_{CP}$ describes the rigid kinematic model between the DOFs of the generic internal node C and the m junction DOFs of the node P. In this example $m = 6$, thus:

$$\tau_{CP} = \begin{bmatrix}\mathbf{I}_{33} & {}^*\mathbf{CP}\\ \mathbf{0}_{33} & \mathbf{I}_{33}\end{bmatrix} \tag{9}$$

where ${}^*\mathbf{CP}$ is the skew-symmetric matrix associated with the vector from C to P. Note that τ_{CP} corresponds exactly to the junction modes matrix $\boldsymbol{\Psi}_{ij}$ of the previous section without any need of inversion as in Eq. (5). By using Eq. (8) and all the previous considerations, Eq. (1) takes the form:

$$\begin{bmatrix}\mathbf{M}_{\mathrm{ff}} & \mathbf{M}_{\mathrm{fr}}\\ \mathbf{M}_{\mathrm{fr}}^{\mathrm{T}} & \mathbf{M}_{\mathrm{rr}}\end{bmatrix}\begin{bmatrix}\widetilde{\ddot{\mathbf{u}}}_i\\ \ddot{\mathbf{u}}_P\end{bmatrix} + \begin{bmatrix}\mathbf{C}_{ii} & \widetilde{\mathbf{C}}_{ij}\\ \widetilde{\mathbf{C}}_{ji} & \widetilde{\mathbf{C}}_{jj}\end{bmatrix}\begin{bmatrix}\widetilde{\dot{\mathbf{u}}}_i\\ \dot{\mathbf{u}}_P\end{bmatrix} + \begin{bmatrix}\mathbf{K}_{ii} & \mathbf{0}_{ij}\\ \mathbf{0}_{ji} & \mathbf{0}_{jj}\end{bmatrix}\begin{bmatrix}\widetilde{\mathbf{u}}_i\\ \mathbf{u}_P\end{bmatrix} = \begin{bmatrix}\mathbf{F}_{\mathcal{L}_{i+1}/\mathcal{L}_i,C}\\ \boldsymbol{\tau}_{CP}^{\mathrm{T}}\mathbf{F}_{\mathcal{L}_{i+1}/\mathcal{L}_i,C} - \mathbf{F}_{\mathcal{L}_i/\mathcal{L}_{i-1},P}\end{bmatrix} \tag{10}$$

where $\mathbf{M}_{\mathrm{rr}}$ is the rigid body matrix associated with $\mathcal{L}_i$ seen from the node P and $\mathbf{M}_{\mathrm{ff}}$ and $\mathbf{M}_{\mathrm{fr}}$ are respectively the mass sub-matrix associated with the flexible DOFs $\widetilde{\mathbf{u}}_i$ and the flexible-rigid cross-coupling sub-matrix. A modal analysis is performed with the new system in Eq. (10) and, noticing that the junction modes matrix $\boldsymbol{\Psi}_{ij} = \mathbf{0}_{ij}$ (from Eq. (5)), Eq. (7) is written as:

$$\begin{bmatrix}\mathbf{I}_{kk} & \mathbf{L}_{kP}\\ \mathbf{L}_{Pk} & \mathbf{M}_{\mathrm{rr}}\end{bmatrix}\begin{bmatrix}\ddot{\boldsymbol{\eta}}_k\\ \ddot{\mathbf{u}}_P\end{bmatrix} + \begin{bmatrix}\mathbf{c}_{kk} & \mathbf{0}_{kj}\\ \mathbf{0}_{jk} & \mathbf{0}_{jj}\end{bmatrix}\begin{bmatrix}\dot{\boldsymbol{\eta}}_k\\ \dot{\mathbf{u}}_P\end{bmatrix} + \begin{bmatrix}\mathbf{k}_{kk} & \mathbf{0}_{kj}\\ \mathbf{0}_{jk} & \mathbf{0}_{PP}\end{bmatrix}\begin{bmatrix}\boldsymbol{\eta}_k\\ \mathbf{u}_P\end{bmatrix} = \begin{bmatrix}\boldsymbol{\Phi}_{kC}\mathbf{F}_{\mathcal{L}_{i+1}/\mathcal{L}_i,C}\\ \tau_{CP}^{\mathrm{T}}\mathbf{F}_{\mathcal{L}_{i+1}/\mathcal{L}_i,C} - \mathbf{F}_{\mathcal{L}_i/\mathcal{L}_{i-1},P}\end{bmatrix} \tag{11}$$

where now:

- $\mathbf{L}_{kP} = \boldsymbol{\Phi}_{ki}\mathbf{M}_{\mathrm{fr}}$
- $\mathbf{c}_{kk} = \mathrm{diag}(2\zeta_k\omega_k)$
- $\mathbf{k}_{kk} = \mathrm{diag}(\omega_k^2)$

By using Eq. (11) and by computing the acceleration vector $\ddot{\mathbf{u}}_C$ at point C (thanks to Eq. (8)) and the modal superposition in Eq. (6):

$$\ddot{\mathbf{u}}_C = \boldsymbol{\Phi}_{Ck}\ddot{\eta}_k + \tau_{CP}\ddot{\mathbf{u}}_P \tag{12}$$

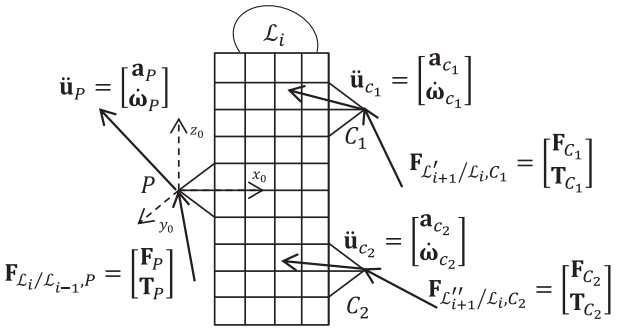

Fig. 4. *i*-th flexible appendage of a complex sub-structured body with two child sub-structures.

the state space representation of the TITOP model $\mathcal{M}_{PC}^{\mathcal{L}_i}(s)$ is finally expressed as:

$$\left[\begin{array}{c} \dot{\eta}_k \\ \ddot{\eta}_k \\ \hline \ddot{\mathbf{u}}_C \\ \mathbf{F}_{\mathcal{L}_i/\mathcal{L}_{i-1},P} \end{array}\right] = \left[\begin{array}{cc|cc} \mathbf{0}_{kk} & \mathbf{I}_{kk} & \mathbf{0}_{kC} & \mathbf{0}_{kP} \\ -\mathbf{k}_{kk} & -\mathbf{c}_{kk} & \boldsymbol{\Phi}_{kC} & -\mathbf{L}_{kP} \\ \hline -\boldsymbol{\Phi}_{Ck}\mathbf{k}_{kk} & -\boldsymbol{\Phi}_{Ck}\mathbf{c}_{kk} & \boldsymbol{\Phi}_{Ck}\boldsymbol{\Phi}_{kC} & (\tau_{CP} - \boldsymbol{\Phi}_{Ck}\mathbf{L}_{kP}) \\ \mathbf{L}_{Pk}\mathbf{k}_{kk} & \mathbf{L}_{Pk}\mathbf{c}_{kk} & (\tau_{CP} - \boldsymbol{\Phi}_{Ck}\mathbf{L}_{kP})^{\mathrm{T}} & \mathbf{L}_{Pk}\mathbf{L}_{kP} - \mathbf{M}_{\mathrm{rr}} \end{array}\right] \left[\begin{array}{c} \eta_k \\ \dot{\eta}_k \\ \hline \mathbf{F}_{\mathcal{L}_{i+1}/\mathcal{L}_i,C} \\ \ddot{\mathbf{u}}_P \end{array}\right] \tag{13}$$

This model, conceived with the clamped-free condition, is useful to study any other kind of boundary configuration as proved in Ref. [33] thanks to the invertibility of all of its 12 input-output channels. Moreover the TITOP model allows us to directly link several sub-structures of an open/closed chain-like complex body.

Note that the same formulation is also suitable for TITOP model obtained by the results provided by MSC/Nastran dynamic analysis as well. The channel inversion operation will be more extensively analyzed in Sec. 3, where a possible source of error will be highlighted.

2.2.1. Extension to the NINOP approach

The model in Eq. (13) can be easily extended to the case in which the flexible appendage $\mathcal{L}_i$ is connected to several child sub-structures like the example in Fig. 4, where a configuration with two child sub-structures is illustrated. Note that there must be a single junction node P in order to build the TITOP model. Thus if $\mathcal{L}_i$ has more than one parent, only one has to be chosen as clamped. The other ones will be considered as child nodes in free boundary condition for the model synthesis. Then the appropriate boundary conditions will be set on these nodes thanks to the inversion on the respective model channels.

In this example the three-input three-output port state-space realization $\mathcal{M}_{PC_1C_2}^{\mathcal{L}_i}(s)$ is written as:

$$\left[\begin{array}{c} \dot{\eta}_k \\ \ddot{\eta}_k \\ \hline \ddot{\mathbf{u}}_{C_1} \\ \ddot{\mathbf{u}}_{C_2} \\ \mathbf{F}_{\mathcal{L}_i/\mathcal{L}_{i-1},P} \end{array}\right] = \left[\begin{array}{cc|ccc} \mathbf{0}_{kk} & \mathbf{I}_{kk} & \mathbf{0}_{kC_1} & \mathbf{0}_{kC_2} & \mathbf{0}_{kP} \\ -\mathbf{k}_{kk} & -\mathbf{c}_{kk} & \boldsymbol{\Phi}_{kC_1} & \boldsymbol{\Phi}_{kC_2} & -\mathbf{L}_{kP} \\ \hline -\boldsymbol{\Phi}_{C_1k}\mathbf{k}_{kk} & -\boldsymbol{\Phi}_{C_1k}\mathbf{c}_{kk} & \boldsymbol{\Phi}_{C_1k}\boldsymbol{\Phi}_{kC_1} & \boldsymbol{\Phi}_{C_1k}\boldsymbol{\Phi}_{kC_2} & (\tau_{C_1P} - \boldsymbol{\Phi}_{C_1k}\mathbf{L}_{kP}) \\ -\boldsymbol{\Phi}_{C_2k}\mathbf{k}_{kk} & -\boldsymbol{\Phi}_{C_2k}\mathbf{c}_{kk} & \boldsymbol{\Phi}_{C_2k}\boldsymbol{\Phi}_{kC_1} & \boldsymbol{\Phi}_{C_2k}\boldsymbol{\Phi}_{kC_2} & (\tau_{C_2P} - \boldsymbol{\Phi}_{C_2k}\mathbf{L}_{kP}) \\ \mathbf{L}_{Pk}\mathbf{k}_{kk} & \mathbf{L}_{Pk}\mathbf{c}_{kk} & (\tau_{C_1P} - \boldsymbol{\Phi}_{C_1k}\mathbf{L}_{kP})^{\mathrm{T}} & (\tau_{C_2P} - \boldsymbol{\Phi}_{C_2k}\mathbf{L}_{kP})^{\mathrm{T}} & \mathbf{L}_{Pk}\mathbf{L}_{kP} - \mathbf{M}_{\mathrm{rr}} \end{array}\right] \left[\begin{array}{c} \eta_k \\ \dot{\eta}_k \\ \hline \mathbf{F}_{\mathcal{L}'_{i+1}/\mathcal{L}_i,C_1} \\ \mathbf{F}_{\mathcal{L}''_{i+1}/\mathcal{L}_i,C_2} \\ \ddot{\mathbf{u}}_P \end{array}\right]$$

The same pattern is easily adapted to N-input N-output port models.

3. The problem of inversion

Let us see an illustrative example of inversion to obtain a dynamic model of a complex multibody structure in tree-like configuration. As said before, if $\ddot{\mathbf{u}}_P = \mathbf{0}$ and $\mathbf{F}_{\mathcal{L}_{i+1}/\mathcal{L}_i,C} = 0$ in the model $\mathcal{M}_{PC}^{\mathcal{L}_i}(s)$ of Eq. (13), the appendage is in clamped-free condition. Thanks to the fact that a residual mass of the sub-structure $\mathcal{L}_i$ is associated with nodes P and C by FEM synthesis, all the 12 input-output channels are invertible. The single-channel inversion procedure is described in Appendix 1 of [33].

If the inverted channels are contained in a vector called $\mathbf{Y}$, the resulting model will be denoted $\left[\mathcal{M}_{PC}^{\mathcal{L}_i}\right]^{-1\mathbf{Y}}(s)$. If for example $\mathbf{Y} = \begin{bmatrix}2 & 4 & 8\end{bmatrix}$, $\left[\mathcal{M}_{PC}^{\mathcal{L}_i}\right]^{-1\mathbf{Y}}(s)$ is the model obtained by $\mathcal{M}_{PC}^{\mathcal{L}_i}$ by inverting the channels 2, 4 and 8.

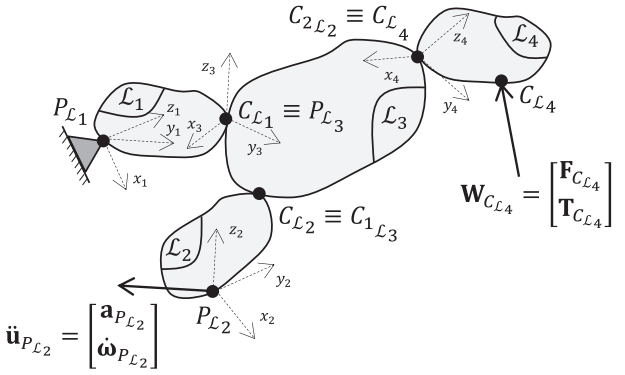

Fig. 5. Tree-like multibody system.

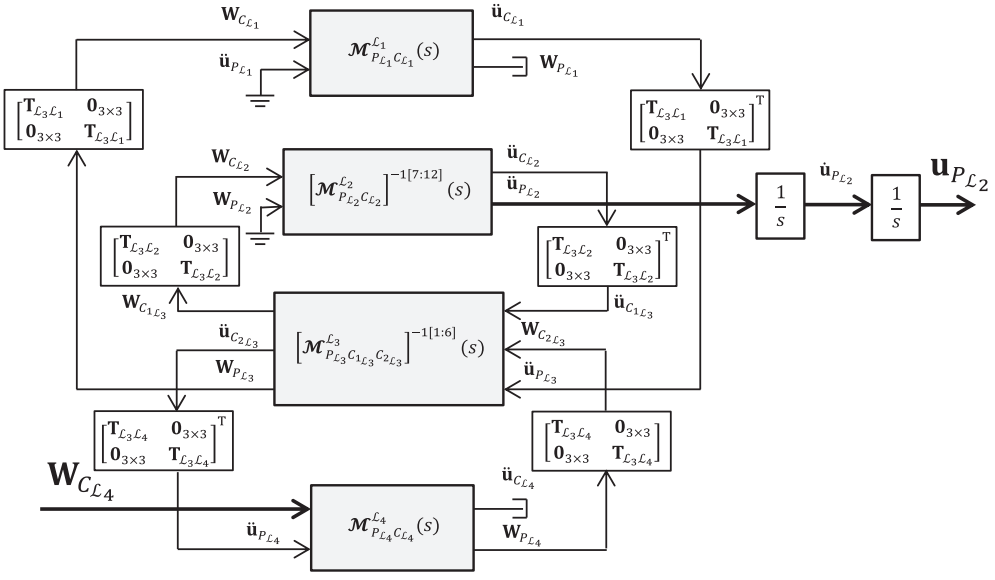

Fig. 6. Block diagram model of the tree-like multibody system of Fig. 5.

Fig. 5 shows a structure with four flexible sub-structures interconnected in tree-like chain by the element $\mathcal{L}_3$. The entire structure is clamped at the point $P_{\mathcal{L}_1}$ of the substructure $\mathcal{L}_1$ and a wrench $\mathbf{W}_{C_{\mathcal{L}_4}}$ acts at the point $C_{\mathcal{L}_4}$ of the sub-structure $\mathcal{L}_4$. The objective is to compute the transfer function between the wrench $\mathbf{W}_{C_{\mathcal{L}_4}}$ and the displacement (linear and angular) $\mathbf{u}_{P_{\mathcal{L}_2}}$ of the point $P_{\mathcal{L}_2}$ of the sub-structure $\mathcal{L}_2$.

Assuming that the TITOP models $\mathcal{M}^{\mathcal{L}_1}_{P_{\mathcal{L}_1}C_{\mathcal{L}_1}}(s)$, $\mathcal{M}^{\mathcal{L}_2}_{P_{\mathcal{L}_2}C_{\mathcal{L}_2}}(s)$, $\mathcal{M}^{\mathcal{L}_4}_{P_{\mathcal{L}_4}C_{\mathcal{L}_4}}(s)$ and the NINOP model $\mathcal{M}^{\mathcal{L}_3}_{P_{\mathcal{L}_3}C_{1_{\mathcal{L}_3}}C_{2_{\mathcal{L}_3}}}(s)$ have already been computed and considering the four inertial reference frames $\mathcal{R}_{\mathcal{L}_1} = (P_{\mathcal{L}_1}, \mathbf{x}_1, \mathbf{y}_1, \mathbf{z}_1)$, $\mathcal{R}_{\mathcal{L}_2} = (P_{\mathcal{L}_2}, \mathbf{x}_2, \mathbf{y}_2, \mathbf{z}_2)$, $\mathcal{R}_{\mathcal{L}_3} = (P_{\mathcal{L}_3}, \mathbf{x}_3, \mathbf{y}_3, \mathbf{z}_3)$ and $\mathcal{R}_{\mathcal{L}_4} = (P_{\mathcal{L}_4}, \mathbf{x}_4, \mathbf{y}_4, \mathbf{z}_4)$ and the three direction cosine matrices $\mathbf{T}_{\mathcal{L}_3\mathcal{L}_1}$ (the matrix components of unitary vectors $\mathbf{x}_1, \mathbf{y}_1, \mathbf{z}_1$ in $\mathcal{R}_{\mathcal{L}_3}$), $\mathbf{T}_{\mathcal{L}_3\mathcal{L}_2}$ (between $\mathcal{R}_{\mathcal{L}_3}$ and $\mathcal{R}_{\mathcal{L}_1}$) and $\mathbf{T}_{\mathcal{L}_3\mathcal{L}_4}$ (between $\mathcal{R}_{\mathcal{L}_3}$ and $\mathcal{R}_{\mathcal{L}_4}$), Fig. 6 shows the block representation of the model of the structure with the four flexible sub-structures.

The example has shown how the computation of inverse models is useful. The operating procedure to compute TITOP or NINOP inverse models is thus important and needs to be studied specifically. In particular, when the direct models are established from finite elements, the modal base used to build the models and the possible mode truncation will be discussed.

3.1. Direct model of a uniform beam

Before computing the inverse model, let us start by analysing the direct model of a uniform beam in pure flexion. The beam is characterized by a density ρ, a Young Modulus E, a length L, a cross-sectional area S and a second moment of area J about the y axis. The TITOP model can be computed by integrating the results provided by three different FEM analyses into three TITOP elements:

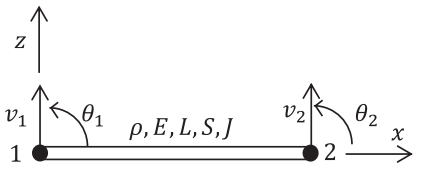

Fig. 7. The beam finite element under bending in the *xz* plane.

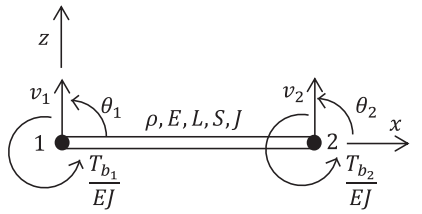

Fig. 8. The beam finite super-element under bending in the *xz* plane.

Table 1
Clamped-free beam 1st mode comparison with Euler-Bernoulli theory. Frequencies are unit-normalized by $\sqrt{\frac{EJ}{\rho SL^4}}$.

Euler - Bernoulli clamped-free beam 1st mode: $\omega_{1\text{ref}} = 3.5160$						
Elements	Beam		Super-Beam		Nastran	
	DOFs	ω_1	DOFs	ω_1	DOFs	ω_1
1	2	3.5327	4	3.5160	2	3.5327
2	4	3.5177	7	3.5160	4	3.5177
3	6	3.5164	10	3.5160	6	3.5164
4	8	3.5161	13	3.5160	8	3.5161
5	10	3.5161	16	3.5160	10	3.5161
6	12	3.5160	19	3.5160	12	3.5160

1. The classical beam element (Fig. 7) with two DOFs for each node (the deflection v and the angle of deflection θ). It is a polynomial model of degree 3;
2. The super-element based on the model used in Ref. [33] and introduced by Ref. [29] (Fig. 8). For this case, the beam model consists in a polynomial model of degree 5 with three DOFs for each of the two boundary nodes (the deflection, the angle of deflection and the double derivative of deflection $\frac{\partial^2 v}{\partial x^2}(x,t) = \frac{T_b(x,t)}{EJ}$, where $T_b(x,t)$ is the bending moment at abscissa x) in planar flexion;
3. The MSC/Nastran CBEAM element. As said before, in practical industrial applications where complex FEM mesh is mandatory to have reliable results, the number of DOFs of the entire structure is really huge and the model is truncated. A FEM toolbox has been developed with Matlab to integrate all these results. In particular an interface has been elaborated in order to recover all the modal parameters needed in Eq. (7) from MSC/Nastran *f06* analysis file and to compute the TITOP model from the equations of Section 2.2.

According to the MSC/Nastran model the default value for the element beam (CBEAM) mass matrix is the lumped mass, that contains only the uncoupled, translational components of mass. The use of this mass is strongly discouraged both in terms of accuracy of results and loss of a certain number of modes. The latter fact causes single-channel inversion problems as shown hereafter. The use of the so called *coupled mass matrix* makes it possible to recover all the modes expected from the number of the complete set of DOFs. However it is not exactly the consistent mass matrix $\mathbf{M}_e$ analytically obtained. Two terms of this matrix are in fact different [35]: the mass in the axial direction is the lumped mass and the torsional inertia is the lumped inertia.

The first four frequencies of the three TITOP models are compared with the results provided by the Euler-Bernoulli beam theory for a clamped-free configuration while considering the entire modal basis. The results for the four direct frequencies are summarized in Tables 1–4, where DOFs is referred to the internal DOFs. Note that, for the Super-Beam element, the DOF relative to the double derivative of deflection of the clamped node is in free condition.

Notice that the results provided by the classical beam element and the MSC/Nastran beam element (in planar case: 2 DOFs for each node) are the same. The beam super-element has more DOFs than the other two elements, thus a small number of elements is needed to reach a determinate level of accuracy. It allows us to develop less complex dynamic models with a small number of states (the number of states is equal to the double of the internal DOFs) while reaching high levels of accuracy.

Table 2
Clamped-free beam 2nd mode comparison with Euler-Bernoulli theory. Frequencies are unit-normalized by $\sqrt{\frac{EJ}{\rho SL^4}}$.

Euler - Bernoulli clamped-free beam 2nd mode: $\omega_{2\text{ref}} = 22.0345$						
Elements	Beam		Super-Beam		Nastran	
	DOFs	ω_2	DOFs	ω_2	DOFs	ω_2
1	2	34.8069	4	22.1578	2	34.8069
2	4	22.2215	7	22.0347	4	22.2215
3	6	22.1069	10	22.0345	6	22.1069
4	8	22.0602	13	22.0345	8	22.0602
5	10	22.0455	16	22.0345	10	22.0455
6	12	22.0399	19	22.0345	12	22.0399
7	14	22.0375	22	22.0345	14	22.0375
8	16	22.0362	25	22.0345	16	22.0362
9	18	22.0356	28	22.0345	18	22.0356
10	20	22.0352	31	22.0345	20	22.0352

Table 3
Clamped-free beam 3rd mode comparison with Euler-Bernoulli theory. Frequencies are unit-normalized by $\sqrt{\frac{EJ}{\rho SL^4}}$.

Euler - Bernoulli clamped-free beam 3rd mode: $\omega_{3\text{ref}} = 61.6972$						
Elements	Beam		Super-Beam		Nastran	
	DOFs	ω_3	DOFs	ω_3	DOFs	ω_3
1	2	–	4	63.3466	2	–
2	4	75.1571	7	61.8308	4	75.1571
3	6	62.4660	10	61.6984	6	62.4660
4	8	62.1749	13	61.6975	8	62.1749
5	10	61.9188	16	61.6973	10	61.9188
6	12	61.8101	19	61.6972	12	61.8101
7	14	61.760	22	61.6972	14	61.760
8	16	61.7347	25	61.6972	16	61.7347
9	18	61.7209	28	61.6972	18	61.7209
10	20	61.7129	31	61.6972	20	61.7129

Table 4
Clamped-free beam 4th mode comparison with Euler-Bernoulli theory. Frequencies are unit-normalized by $\sqrt{\frac{EJ}{\rho SL^4}}$.

Euler - Bernoulli clamped-free beam 4th mode: $\omega_{4\text{ref}} = 120.9019$						
Elements	Beam		Super-Beam		Nastran	
	DOFs	ω_4	DOFs	ω_4	DOFs	ω_4
1	2	–	4	281.5962	2	–
2	4	218.1380	7	122.5912	4	218.1380
3	6	140.6711	10	121.0851	6	140.6711
4	8	122.6576	13	120.9057	8	122.6576
5	10	122.3197	16	120.9036	10	122.3197
6	12	121.6810	19	120.9023	12	121.6810
7	14	121.3483	22	120.9020	14	121.3483
8	16	121.1727	25	120.9019	16	121.1727
9	18	121.0748	28	120.9019	18	121.0748
10	20	121.0171	31	120.9019	20	121.0171

3.2. Inverse model and modal basis truncation

In Ref. [33] the inversion of the TITOP model $\mathcal{M}^{\mathcal{L}}_{PC}(s)$ (with P and C as boundary nodes) of an homogeneous beam was proven: the first two natural frequencies obtained by $\mathcal{M}^{\mathcal{L}}_{PC}(s)$ (clamped-free configuration) and its inverse $\left[\mathcal{M}^{\mathcal{L}}_{PC}\right]^{-1}(s)$ (free-clamped configuration) are the same. Note that this condition is valid only if the geometric and structural properties are symmetric with

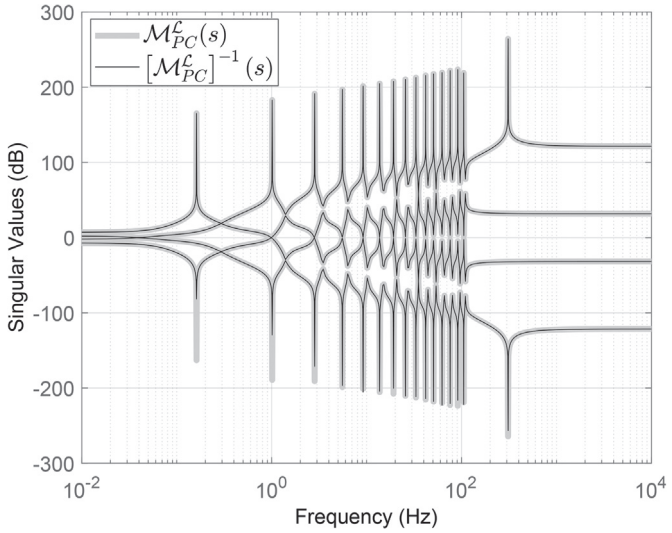

Fig. 9. The four Singular Values plot for a clamped-free uniform beam obtained from the direct model $\mathcal{M}^{\mathcal{L}}_{PC}(s)$ and its inverse $\left[\mathcal{M}^{\mathcal{L}}_{PC}\right]^{-1}(s)$.

respect to midpoint. The question now arises for the inversion of the TITOP model obtained from Nastran FEM analysis.

A way to verify the fact that the direct model $\mathcal{M}^{\mathcal{L}}_{PC}(s)$ (clamped-free configuration) and its inverse model $\left[\mathcal{M}^{\mathcal{L}}_{PC}\right]^{-1}(s)$ (free-clamped configuration) of a uniform beam have the same set of modal frequency is to analyze the frequency domain response of the singular values of $\mathcal{M}^{\mathcal{L}}_{PC}(\mathrm{j}\omega)$ in Eq. (13) while neglecting the damping term. The singular value responses according to the frequency ω in logarithmic scale (thanks to the Matlab function `sigma`) has to be symmetric w.r.t. the frequency axis since:

$$\sigma_i\left(\mathcal{M}^{\mathcal{L}}_{PC}(\mathrm{j}\omega)\right) = \sigma_i\left(\left[\mathcal{M}^{\mathcal{L}}_{PC}\right]^{-1}(\mathrm{j}\omega)\right) \quad \forall\, i \tag{14}$$

The singular values of the inverse model $\left[\mathcal{M}^{\mathcal{L}}_{PC}\right]^{-1}(s)$ are exactly the inverse singular values of $\mathcal{M}^{\mathcal{L}}_{PC}(s)$. In practice and for illustration, by building the model of a clamped-free beam with five super-element beams, the plot of Fig. 9 shows that the peaks and the wells of $\left[\mathcal{M}^{\mathcal{L}}_{PC}\right]^{-1}(s)$ occur at the same frequencies of those of $\mathcal{M}^{\mathcal{L}}_{PC}(s)$. Note that the direct TITOP model for the beam working in pure flexion in the plane (x,z) (see Fig. 8) has 4 inputs:

- the force along z-axis and the torque around y-axis applied to the beam at the point C;
- the linear acceleration along z-axis and the angular acceleration around y-axis of the point P

and 4 outputs:

- the linear acceleration along z-axis and the angular acceleration around y-axis of the point C;
- the force along z-axis and the torque around y-axis applied by the beam at the point P.

Let us now consider a model obtained by commercial FEM analysis. One issue of the FEM approach is to limit the computational cost and data storage. It is usually common practice to truncate the modal basis, by removing the less significant modes. The final set of modal solutions η_k is thus truncated to a smaller set η_q, with $q < k$, obtained by removing the higher frequency modes since their participation in response to the total low frequency excitation is negligible [36].

This section will now show why the modal truncation is detrimental for TITOP single-channel inversion. Let us consider a TITOP model $\mathcal{M}^{\mathcal{L}}_{PC}(s)$ of a uniform beam analyzed by only two element beams. The natural frequencies embedded in this system are four. If now a truncated model $\mathcal{M}^{\mathcal{L}}_{PC_{\mathrm{tru,\,2}}}(s)$, taking the contribution of only the first two modes, is considered, the computed natural frequencies are resumed in Table 5. A comparison with the complete model $\mathcal{M}^{\mathcal{L}}_{PC}(s)$ and a MSC/Nastran beam model (with two CBEAM elements and four modes) is done. Fig. 10 finally compares the singular values plot of the three direct models.

Two observations can be made:

1. Let us define the frequency relative error defined as $\Delta\omega_i\% = 100\frac{|\omega_i^{\mathrm{inv}} - \omega_i^{\mathrm{dir}}|}{\omega_i^{\mathrm{dir}}}$, with ω_i^{dir} (ω_i^{inv}) frequency of the mode i of the direct (inverse) model. For the model synthesized by MSC/Nastran is equal to 0.09% for the first mode and 0.03% for the second one. These extremely small errors can be further reduced if a finer mesh is used. These errors can also be visualized

Table 5
TITOP Direct (clamped-free) and inverse (free-clamped) first two normal frequencies for a uniform beam: comparison between the complete model $\mathcal{M}^{\mathcal{L}}_{PC}(s)$, the truncated one $\mathcal{M}^{\mathcal{L}}_{PC_{\text{tru},2}}(s)$ and a MSC/Nastran TITOP beam model $\mathcal{M}^{\mathcal{L}}_{PC_{\text{MSC}}}(s)$ (all the modal basis is taken into account: no truncation performed). Frequencies are unit-normalized by $\sqrt{\frac{EJ}{\rho S l^4}}$.

Mode	$\mathcal{M}^{\mathcal{L}}_{PC}(s)$	$\left[\mathcal{M}^{\mathcal{L}}_{PC}\right]^{-1}(s)$	$\mathcal{M}^{\mathcal{L}}_{PC_{\text{tru},2}}(s)$	$\left[\mathcal{M}^{\mathcal{L}}_{PC_{\text{tru},2}}\right]^{-1}(s)$	$\mathcal{M}^{\mathcal{L}}_{PC_{\text{MSC}}}(s)$	$\left[\mathcal{M}^{\mathcal{L}}_{PC_{\text{MSC}}}\right]^{-1}(s)$
1	3.5177	3.5177	3.5177	5.7879	3.5177	3.5144
2	22.2215	22.2215	22.2215	72.2116	22.2215	22.2272

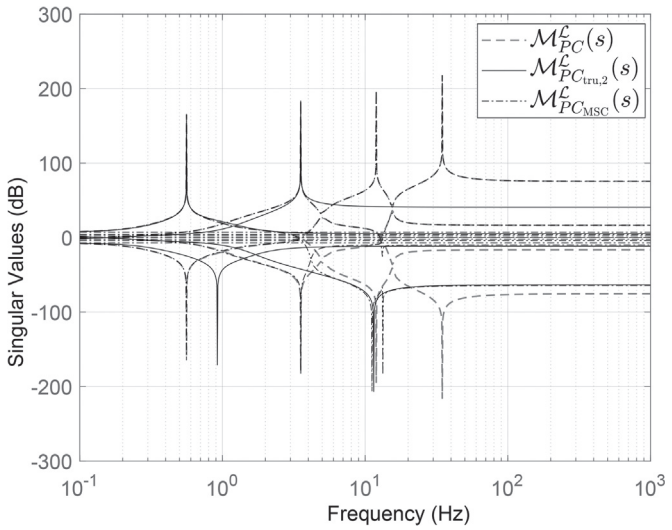

Fig. 10. Singular Values plot for a clamped-free uniform beam: comparison between the complete model $\mathcal{M}^{\mathcal{L}}_{PC}(s)$, the truncated one $\mathcal{M}^{\mathcal{L}}_{PC_{\text{tru},2}}(s)$ and a MSC/Nastran TITOP beam $\mathcal{M}^{\mathcal{L}}_{PC_{\text{MSC}}}(s)$.

in Fig. 10 where $\mathcal{M}^{\mathcal{L}}_{PC_{\text{MSC}}}(s)$ singular values are not perfectly symmetric as $\mathcal{M}^{\mathcal{L}}_{PC}(s)$ ones;

2. The frequency relative error for the truncated inverse model $\left[\mathcal{M}^{\mathcal{L}}_{PC_{\text{tru},2}}\right]^{-1}(s)$ is catastrophically erroneous: 64.54% for the first mode and 224.96% for the second one. These errors are caused by a non-compensation of the truncated modes. They are nonetheless unacceptable and the advantage of truncation is lost because of the augmented complexity of the system.

3.2.1. Conclusions on the problem of the inversion of dynamic FEM models

When the inversion of dynamic FEM models is required (to compute models in boundary conditions different from free-clamped conditions or to compute inverse models), the entire modal basis is mandatory and the use of consistent mass matrices is preferable. Only the super-element beam complies with these two requirements. Moreover the classical operation of statically residualizing the response of the truncated modes, used to obtain the good value for the static gain, does not solve the problem of the location of the modes of the inverse model. Note: when only direct dynamic FEM models are required (e.g. for control purposes of clamped-free multibody structures), only a few modes at the lowest frequencies are important. The use of super-element beams to compute FEM models of such structures is not mandatory but gives a high level of precision with a limited set of elements. Another option is to use truncated dynamic FEM models obtained by any commercial software. This promotes the direct use of MSC/Nastran results in the developed toolbox where any kind of elements (even 3-dimensional elements for complex structures) are supported.

This article continues with an extension of the TITOP approach to N-Input N-Output port systems in the particular case of a bending plate. The problem of the augmented system complexity will be addressed.

4. Finite-element plate model in NINOP formulation

In this section a FEM NINOP model is developed for a bending plate. The *thin-plate theory* proposed by Kirchhoff in 1850 has been adopted to formulate plate elements. Note that the goal of this article is not actually to produce really efficient elements but to show the potential of the NINOP approach to provide models easily manageable by control engineers for the purpose of

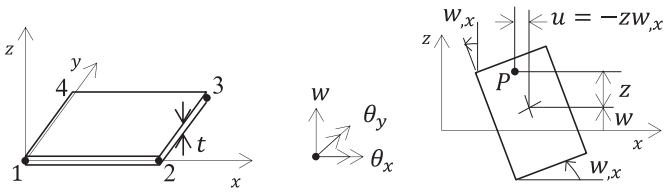

Fig. 11. A four-node plate element: notation and deformed cross-section.

Table 6
Mechanical characteristics of a sample bending plate.

Description	Symbol	Value
Density	ρ	2015 kg/m^3
Young Modulus	E	69.8692 MPa
Shear Modulus	G	22.1615 MPa
Length	l_x	1 m
Width	l_y	1 m
Thickness	t	0.003 m

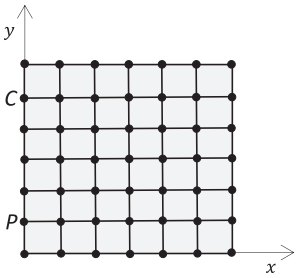

Fig. 12. Mesh of a clamped (in P) -free (in C) plate.

structural design under uncertainty.

A plate element with four nodes is considered with the notations of Fig. 11. Each node has three DOFs: the displacement w along z-axis, the rotation θ_x around x-axis and the rotation θ_y around y-axis. The plate thickness is denoted t. We note $w_{,x} = \frac{\partial w}{\partial x}$ and $w_{,y} = \frac{\partial w}{\partial y}$ the plate surface slopes. For an exhaustive treatment of the Kirchhoff plate theory refer to [37].

As is well known, this element could be incompatible in normal slope: along a shared side (for instance $x = const$), adjacent elements generally display different values of $w_{,x}$. These incompatibilities tend towards zero if the mesh is refined and the element performs satisfactorily.

Table 7
Direct and inverse TITOP models obtained by Kirchhoff element plate ($\mathcal{M}_{\text{TITOP}}(s)$) and MSC/Nastran CQUAD4 element ($\mathcal{M}_{\text{MSC}}(s)$). Frequencies are expressed in rad/s.

Mode	$\mathcal{M}_{\text{TITOP}}(s)$		$\mathcal{M}_{\text{MSC}}(s)$	
	Direct	Inverse	Direct	Inverse
1	8.3932	8.3932	8.2887	9.1241
2	17.0366	17.0366	16.9616	18.2827
3	53.5979	53.5979	53.3940	55.1281
4	108.6055	108.6055	110.8640	114.5049
5	139.0182	139.0182	142.4158	148.1564
6	169.4045	169.4045	173.3120	174.3294
7	201.2494	201.2494	205.2948	210.7449
8	312.0921	312.0921	326.9772	340.4803
9	354.5345	354.5345	376.0121	387.5427
10	368.7387	368.7387	396.7305	396.4752

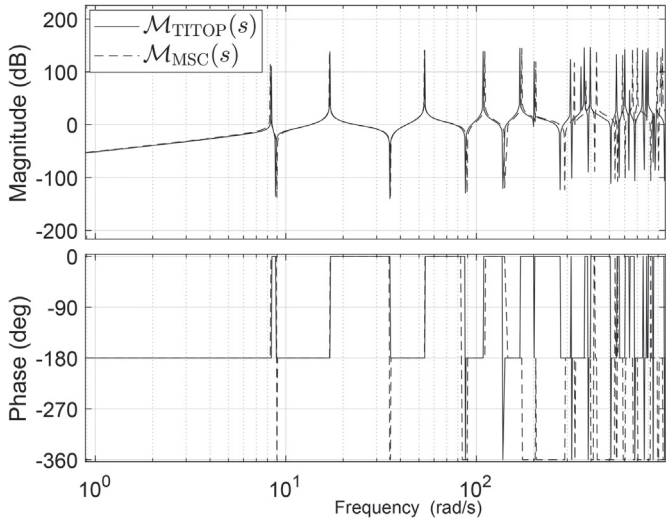

Fig. 13. Bode plot of the direct TITOP models obtained by Kirchhoff element plate ($\mathcal{M}_{\mathrm{TITOP}}(s)$) and MSC/Nastran CQUAD4 element ($\mathcal{M}_{\mathrm{MSC}}(s)$): transfer between the force applied at the point C in z direction and the displacement of point C along z.

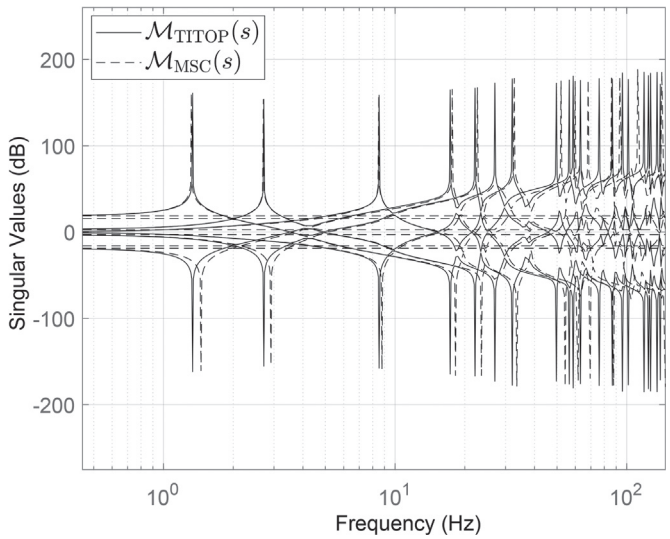

Fig. 14. Singular values plot of the TITOP models obtained by Kirchhoff element plate ($\mathcal{M}_{\mathrm{TITOP}}(s)$) and MSC/Nastran CQUAD4 element ($\mathcal{M}_{\mathrm{MSC}}(s)$).

4.1. An academic example: a uniform bending plate

In this section a simple uniform plate will be studied in TITOP approach both with the Kirchhoff element and with the CQUAD4 element available in MSC/Nastran, based on Mindlin-Reissner theory [38]. For this element transverse shear strains are also taken into account (neglected in Kirchhoff theory). Let us consider the bending plate whose mechanical characteristics are listed in Table 6.

Table 8
Total computational time for the models $\mathcal{M}_{\mathrm{TITOP}}(s)$ and $\mathcal{M}_{\mathrm{MSC}}(s)$.

Time	$\mathcal{M}_{\mathrm{TITOP}}(s)$		$\mathcal{M}_{\mathrm{MSC}}(s)$	
	Direct	Inverse	Direct	Inverse
minimum	6.271 s	4.214 ms	4.176 s	1.001 ms
average	6.574 s	4.720 ms	4.187 s	1.371 ms

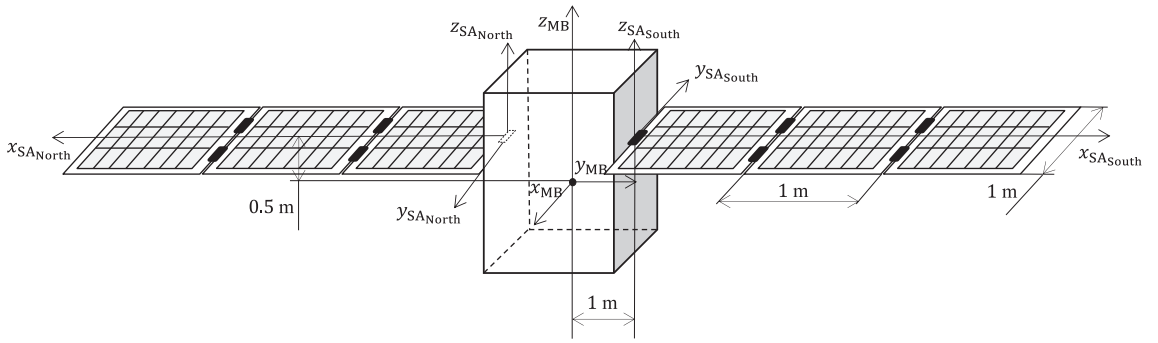

Fig. 15. Reference frames of a spacecraft with two deployable solar panels.

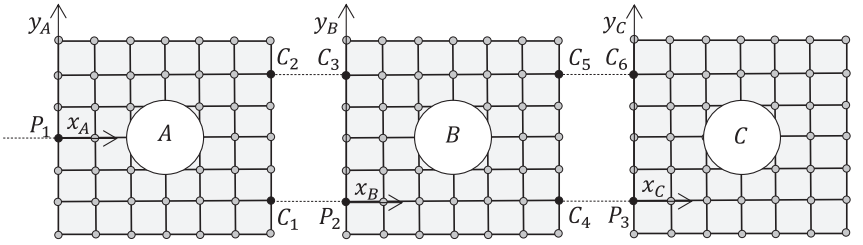

Fig. 16. Finite element mesh for a three plate deployable solar array.

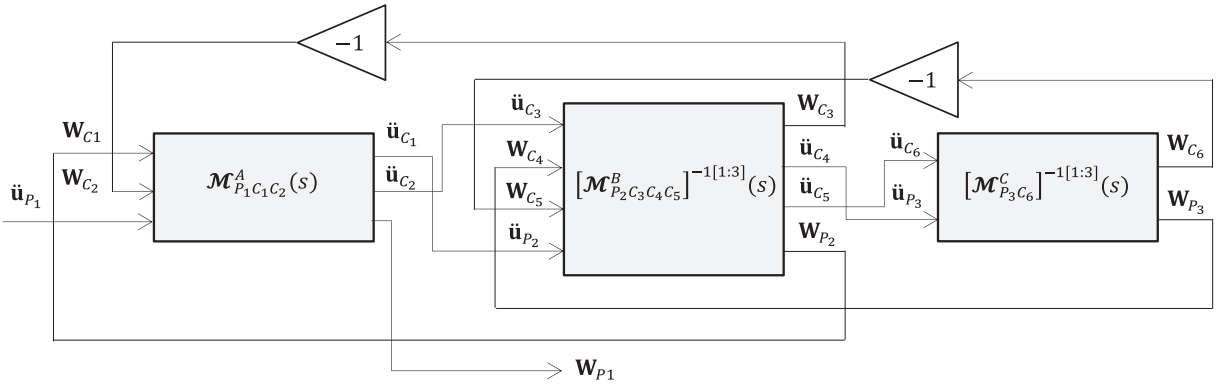

Fig. 17. Block diagram model for a three plate deployable solar array.

A mesh of six plate elements (Fig. 12) in *x* and *y* directions is used to study a plate clamped at the node *P*. All the other nodes are in free condition. All the 6 DOFs of *P* are blocked for the MSC/Nastran model and, for the other nodes, only DOFs 1,2,6 are blocked in order to compare the results of the modal analysis with the developed Kirchhoff element. The goal of the present section is to provide the TITOP model between the clamped node *P* and the free node *C* (Fig. 12). The two nodes have been chosen symmetrically in order to verify the invertibility of the channels. The inverse TITOP model indeed provides the model of the plate clamped in *C* and free in *P*. Since this condition is exactly symmetric to the previous one, the same set of modal frequencies has to be found.

Table 7 gives the results of the first ten modes computed from the direct and inverse TITOP models (clamped in P and free in C) based on the developed Kirchhoff plate (model designed as $\mathcal{M}_{\text{TITOP}}(s)$) and the MSC/Nastran normal mode analysis (model designed as $\mathcal{M}_{\text{MSC}}(s)$). In Fig. 13 the transfer between the force applied at the point *C* in *z* direction and the displacement of point *C* along *z* is shown.

By comparison of the direct and the inverse model (clamped in *C* and free in *P*) in Table 7, notice that the MSC/Nastran CQUAD4 element leads to different results of natural frequencies w.r.t. the direct model while the developed Kirchooff element performs the same results for both models. Moreover the diagram of the singular values for the CQUAD4 element (Fig. 14) is not symmetric as expected for the reasons given in Sec. 3.2. This small difference is caused by two reasons:

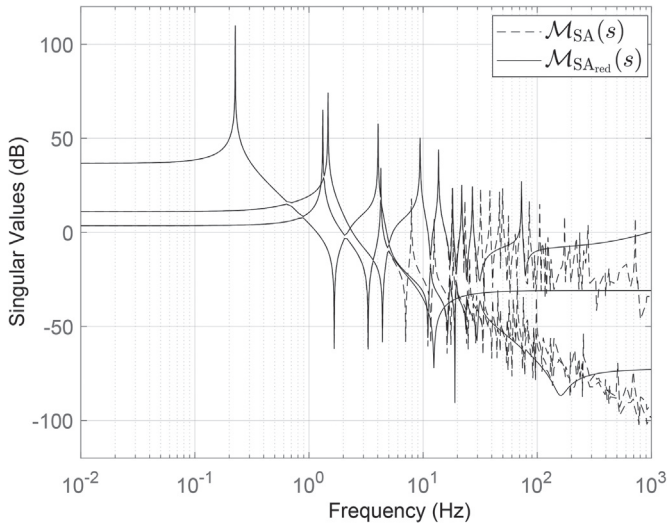

Fig. 18. Singular values plot of the complete ($\mathcal{M}_{SA}(s)$) and reduced model ($\mathcal{M}_{SA_{red}}(s)$) of the solar array.

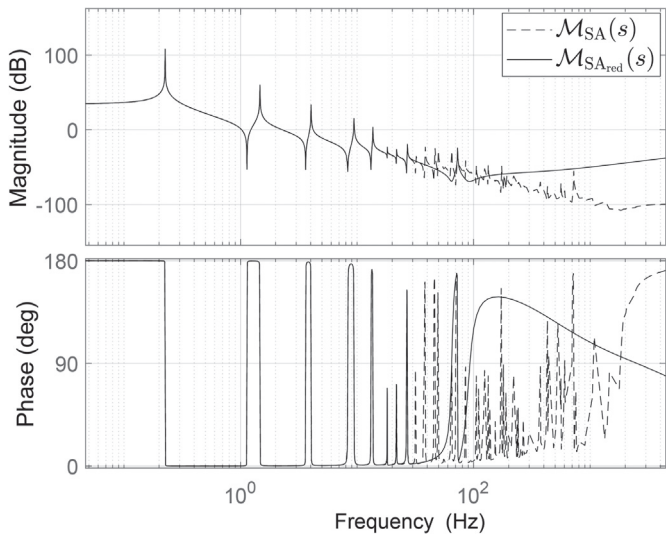

Fig. 19. Bode plot of the transfer between the angular acceleration around SA x-axis of the node P_1 and the corresponding reaction torque at the same point: complete ($\mathcal{M}_{SA}(s)$) and reduced model ($\mathcal{M}_{SA_{red}}(s)$) of the solar array.

1. the use of a *coupled mass matrix* instead of the consistent mass matrix in MSC/Nastran environment;
2. the modal basis truncation: only 48 modes are found by MSC/Nastran SOL 103 instead of the expected 144. A truncation ratio 3 is thus performed.

A short discussion follows on the computation time of the different models. Table 8 resumes the minimum and the average computation times obtained by 100 executions for the direct and the inverse models of $\mathcal{M}_{TITOP}(s)$ and $\mathcal{M}_{MSC}(s)$. Note that the computation times of the direct model $\mathcal{M}_{MSC}(s)$ include 4s taken by the Nastran analysis process. The remaining time is due to the Matlab interface for the reading of the results file and the state-space synthesis. Note that for the computation of the direct model $\mathcal{M}_{TITOP}(s)$ no code optimization has been performed at this stage. Referring to the inverse model, the computation time depends on the number of states of the direct model. $\mathcal{M}_{TITOP}(s)$ has three times the number of states of $\mathcal{M}_{MSC}(s)$ because no modal basis truncation is performed, as remarked before, thus the computation time is larger as shown in Table 8. For both cases (direct and inverse models), the computation time for $\mathcal{M}_{TITOP}(s)$ is acceptable even if it is larger than for $\mathcal{M}_{MSC}(s)$.

Table 9
Spacecraft mechanical characteristics.

	Description	Symbol	Value	Unit
Main Body	Position gravity center	CG_{MB}	$\begin{bmatrix}0 & 0 & 0\end{bmatrix}$	m
	Mass	m_{MB}	100	kg
	Main Inertia in $(CG_{MB}, x_{MB}, y_{MB}, z_{MB})$	$I_{xx_{MB}}, I_{yy_{MB}}, I_{zz_{MB}}$	10,10,20	kg m^2
	Cross Inertia in $(CG_{MB}, x_{MB}, y_{MB}, z_{MB})$	$I_{xy_{MB}}, I_{xz_{MB}}, I_{yz_{MB}}$	0,0,0	kg m^2
SA	Position gravity center in $(P_{SA}, x_{SA}, y_{SA}, z_{SA})$	CG_{SA}	$\begin{bmatrix}1.5 & 0 & 0\end{bmatrix}$	m
	Mass	m_{SA}	18.135	kg
	Main Inertia in $(P_{SA}, x_{SA}, y_{SA}, z_{SA})$	$I_{zz_{SA}}$	55.9163	kg m^2

4.2. A practical application: dynamic model of a satellite with deployable solar arrays

Let us consider the spacecraft in Fig. 15 with two symmetric deployable solar arrays (SA). Each SA is composed of three plates (A, B and C), better represented in Fig. 16. In the same figure the mesh of each plate is shown with the attachment nodes between two panels: the nodes P_i and C_i (corresponding to the interconnection points) employed for the NINOP synthesis are highlighted. The Kirchhoff plate elements are used to get the three dynamic direct models of each panel ($\mathcal{M}^A_{P_1C_1C_2}(s)$, $\mathcal{M}^B_{P_2C_3C_4C_5}(s)$ and $\mathcal{M}^C_{P_3C_6}(s)$), by considering P_i as clamped nodes and C_i as free nodes. Plates like the one studied in Section 4.1 are used for modeling the satellite.

The block diagram of an assembled SA is shown in Fig. 17. Note that for the panels B and C the three channels corresponding to nodes C_3 and C_6 are inverted in order to consider these nodes as clamped for the assembling operation. Moreover the gains -1 are due to the action/reaction principle applied to the definition given to the wrench in the corresponding NINOP direct models. The transfer function between the acceleration vector $\ddot{\mathbf{u}}_{P_1}$ at point P_1 (the attachment point to the spacecraft) and the wrench at the same point is thus directly deduced.

Each of the three sub-panels provides a model with 144 flexible modes and the assembled solar array corresponds to a model with 864 states. There are two ways to model the solar array for control purposes:

1. Model reduction of each singular sub-panels model after inversion of some channels (Fig. 17) and before assembling;
2. Model reduction of the assembled solar array.

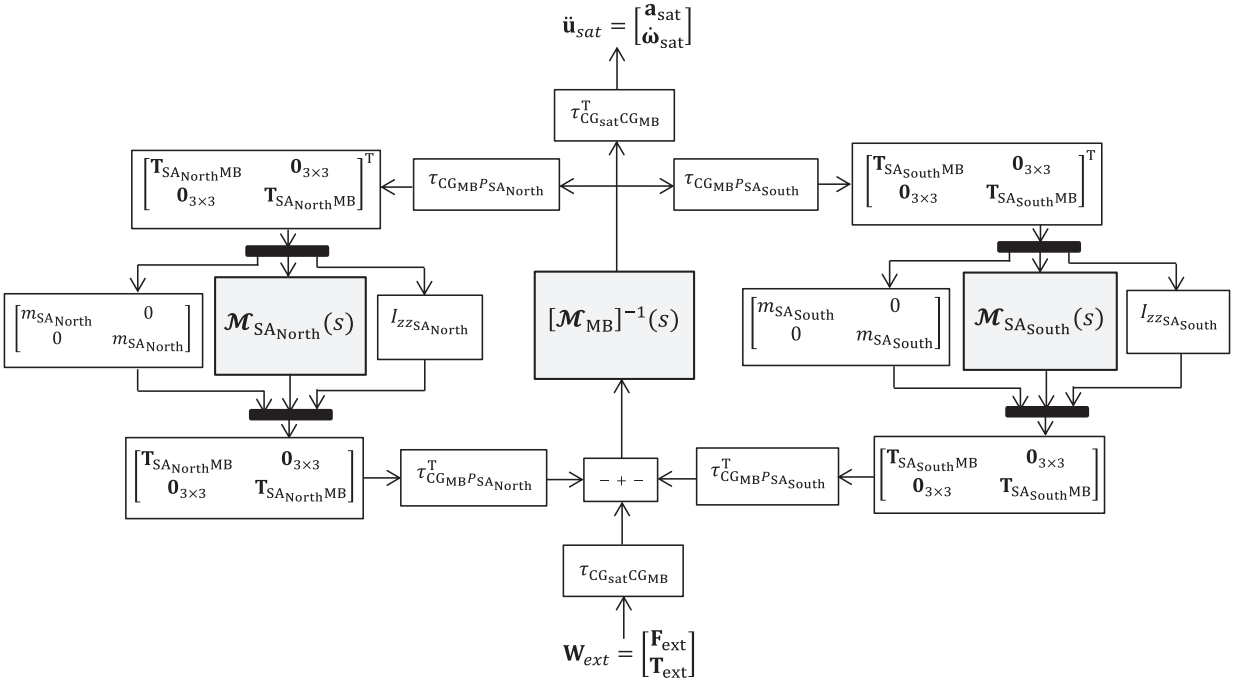

Fig. 20. Block diagram of the complete satellite dynamic model.

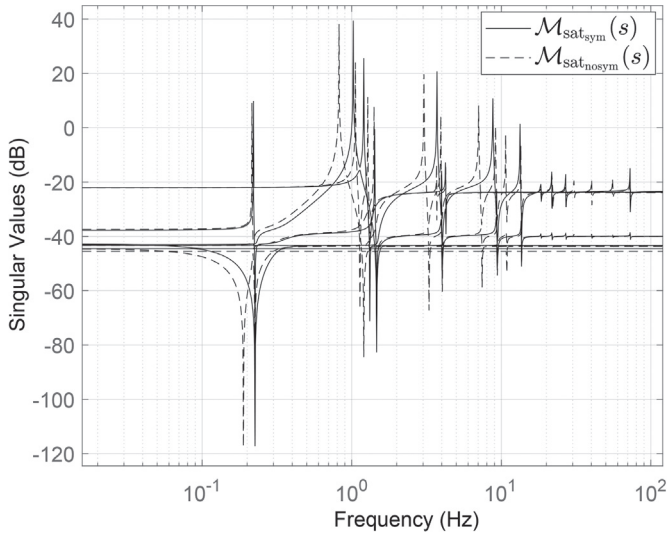

Fig. 21. Singular values of the dynamic model of a spacecraft with symmetric ($\mathcal{M}_{\mathrm{sat}_{\mathrm{sym}}}(s)$) and asymmetric ($\mathcal{M}_{\mathrm{sat}_{\mathrm{nosym}}}(s)$) solar arrays.

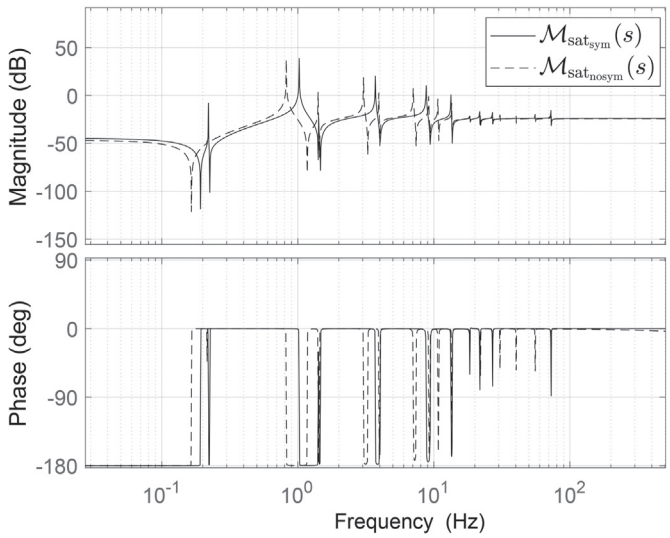

Fig. 22. Bode diagram of the transfer between the external torque acting around satellite x-axis and the angular acceleration provoked around the same axis for a spacecraft with symmetric ($\mathcal{M}_{\mathrm{sat}_{\mathrm{sym}}}(s)$) and asymmetric ($\mathcal{M}_{\mathrm{sat}_{\mathrm{nosym}}}(s)$) solar arrays.

Since for the present example the computational cost related to the assembling of the three sub-panels is not excessive, the second solution is retained. In this way no simplification is done until the assembled model is obtained: this operation prevents any error propagation. A balanced Hankel model reduction (Matlab command `balred`) brings to a reduced model of only 30 states. The singular value plots of the two models (complete and reduced) of the solar array are shown in Fig. 18. The bode plot of the transfer between the angular acceleration around SA x-axis of the node P_1 and the corresponding reaction torque at the same point is shown in Fig. 19 as an example. Note that the reduced model allows to accurately take into account the most important resonant frequencies of the SA until ≈30 Hz.

The entire dynamic model of the spacecraft of Fig. 15 is thus directly deduced. The central body is considered rigid and its mechanical characteristics are resumed in Table 9. Note that this is an example and all the quantities should not be taken as reference. Moreover the solar panels are studied as uniform plates. This is a great approximation because in general they are mainly composed by a honeycomb composite material packed in two thin aluminum layers. This corresponds to anisotropic mechanical properties. For the present study the orthotropic properties are converted to average laminate properties, which are then used in the FE isotropic material definition. The result of this approximation corresponds to the values of Table 6. This approximation is acceptable for a preliminary design.

Another approximation that will be done is that there are only 3 DOFs for the Kirchhoff plate element. For the other ones a rigid-body-like dynamics is assumed between the solar array and the main body.

The complete block diagram model for the satellite is shown in Fig. 20. The synthesis of this diagram directly follows from Ref. [27] and will be not detailed. Note that the inverse dynamic model of the main body $\mathcal{M}_{\mathrm{MB}}(s)$ is the inverse matrix of its rigid mass/inertia matrix, the kinematic blocks $\boldsymbol{\tau}$ allow the kinematic transport of each body to the corresponding interconnection point and the rotation matrices $\mathbf{T}$ relate the different reference frames associated with each body. Finally the block diagram in Fig. 20 provides the transfer function between the external forces/torques $\mathbf{W}_{\mathrm{ext}}$ acting at the center of mass (CG_{sat}) of the entire satellite and its (linear and angular) accelerations $\ddot{\mathbf{u}}_{\mathrm{sat}}$. A double integration of this model allows recovery of the linear displacements and rotations of the spacecraft in the satellite frame.

The great advantage of the model proposed in this paper is that any modification to any parameter (mechanical characteristics of solar panels or of the main body, position of interconnection points) or any uncertainty (asymmetries in mechanical properties) can be easily analyzed without huge computational cost. This makes it possible to perform robust structural and control co-design analysis for the preliminary design of the phases of a mission. If for instance an asymmetry of −20% on the Young's Modulus value and +20% on the density of the sub-panels of the South SA is introduced, the resulting singular value plot is shown in Fig. 21. The transfer between the external torque acting around satellite x-axis and the angular acceleration provoked around the same axis in Fig. 22 shows how the highest resonant peak in the asymmetric configuration moves back to a lower frequency as expected.

Another advantage of such a structured model is the possibility to introduce and analyze the effect of local stiffness and damping corresponding to each deployable mechanism (between points C_1 and P_2, C_2 and C_3, C_4 and P_3, C_5 and C_6 in Fig. 16).

5. Conclusion

This paper addressed the development of an N-input N-output Port dynamic model, based on Finite Element modal analysis, for the resolution of multibody problems. A MATLAB toolbox with self-made elements (bending beams and plates) served as support for testing the TITOP/NINOP approach. An interface with MSC/Nastran normal mode analysis has also been developed to allow computing NINOP dynamic models from the outputs of such software. This study clearly highlighted the potentialities of the present approach, by reducing the analysis of complex structures to a simple interconnection of sub-modules in two steps:

- Extraction of the dynamical content of a body clamped at one node and free at the other ones and extension of the dynamical model to any kind of boundary conditions thanks to simple operation of channel inversion;
- Final models are obtained in the form of block diagrams with a minimal number of states.

The paper also covers the limits of the channel inversion, when a truncation of the direct dynamical model is performed. Self-made elements demonstrated their efficiency in simple test cases with symmetric boundary conditions. The use of a non-consistent mass matrix and truncation in MSC/Nastran models revealed a degree of error in inversion operations, which decreases with a mesh refinement. On the other hand the toolbox interface with MSC/Nastran guarantees precise TITOP/NINOP models when only direct interconnections ports are used (no need of inversion): all types of mesh can be treated in the software developed.

The strength of the TITOP/NINOP approach is the ability to study several configurations in preliminary control/structure design by interconnections of sub-structures in a simple block diagram. A case study of a spacecraft with two flexible solar arrays served as representative benchmark for the application of the present approach. It highlighted the great potentiality of the TITOP/NINOP theory for multibody structures with interconnected repeated modules (i.e. reticulated configurations or a solar array composed by several panels): only one NINOP model needs to be computed and simple interconnections with the same block model finally provide the entire structure dynamics.

Acknowledgment

This work was supported by the European Space Agency (ESA) and Airbus Defence and Space (NPI grant number 4000116571/16/NL/MH). The authors also thank Flávio Luiz Cardoso-Ribeiro for advices and discussions.

Appendix A. Supplementary data

Supplementary data related to this article can be found at https://doi.org/10.1016/j.jsv.2017.11.021

References

[1] C. Cumer, D. Alazard, A. Grynagier, C. Pittet-Mechin, Codesign mechanics/attitude control for a simplified aocs preliminary synthesis, in: 9th International ESA Conference on Guidance, Navigation & Control Systems (GNC 2014), Porto, 2014, pp. 1–9.

[2] N. Guy, D. Alazard, C. Cumer, C. Charbonnel, Dynamic modeling and analysis of spacecraft with variable tilt of flexible appendages, J. Dyn. Syst. Meas. Control 136 (2) (2014) 021020–021020–10, https://doi.org/10.1115/1.4025998.

[3] K.D. Young, Distributed finite-element modeling and control approach for large flexible structures, J. Guidance Control Dyn. 13 (4) (1990) 703–713, https://doi.org/10.2514/3.25389.
[4] H. Holzer, Analysis of Torsional Vibration, Springer, Berlin, 1921.
[5] N. Myklestad, New method of calculating natural modes of coupled bending-torsion vibration of beams, Trans. ASME 67 (1) (1945) 61–67.
[6] X. Rui, B. He, Y. Lu, W. Lu, G. Wang, Discrete time transfer matrix method for multibody system dynamics, Multibody Syst. Dyn. 14 (3) (2005) 317–344, https://doi.org/10.1007/s11044-005-5006-1.
[7] F. Leckie, E. Pestel, Transfer-matrix fundamentals, Int. J. Mech. Sci. 2 (3) (1960) 137–167, https://doi.org/10.1016/0020-7403(60)90001-1.
[8] M. Dokainish, A new approach for plate vibrations: combination of transfer matrix and finite-element technique, J. Eng. Ind. 94 (2) (1972) 526–530, https://doi.org/10.1115/1.3428185.
[9] V. Mucino, V. Pavelic, An exact condensation procedure for chain-like structures using a finite element-transfer matrix approach, J. Mech. Des. 103 (2) (1981) 295–303, https://doi.org/10.1115/1.3254907.
[10] L. Kitis, R. Lindenberg, Natural frequencies and mode shapes of flexible mechanisms by a transfer matrix method, Finite Elem. Anal. Des. 6 (4) (1990) 267–285, https://doi.org/10.1016/0168-874X(90)90020-F.
[11] T. Tan, A. Yousuff, L. Bahar, M. Konstantinidis, A modified finite element-transfer matrix for control design of space structures, Comput. Struct. 36 (1) (1990) 47–55, https://doi.org/10.1016/0045-7949(90)90173-Y.
[12] X. Rui, G. Wang, Y. Lu, L. Yun, Transfer matrix method for linear multibody system, Multibody Syst. Dyn. 19 (3) (2008) 179–207, https://doi.org/10.1007/s11044-007-9092-0.
[13] B. Rong, X. Rui, G. Wang, F. Yang, Discrete time transfer matrix method for dynamics of multibody system with real-time control, J. Sound Vib. 329 (6) (2010) 627–643, https://doi.org/10.1016/j.jsv.2009.09.034.
[14] N. Vijayasree, M. Munjal, On an integrated transfer matrix method for multiply connected mufflers, J. Sound Vib. 331 (8) (2012) 1926–1938, https://doi.org/10.1016/j.jsv.2011.12.003.
[15] X. Rui, J. Zhang, Q. Zhou, Automatic deduction theorem of overall transfer equation of multibody system, Adv. Mech. Eng. 6 (2014) 378047, https://doi.org/10.1155/2014/378047.
[16] W.C. Hurty, Dynamic analysis of structural systems using component modes, AIAA J. 3 (4) (1965) 678–685, https://doi.org/10.2514/3.2947.
[17] R.H. MacNeal, A hybrid method of component mode synthesis, Comput. Struct. 1 (4) (1971) 581–601, https://doi.org/10.1016/0045-7949(71)90031-9.
[18] R.M. Hintz, Analytical methods in component modal synthesis, AIAA J. 13 (8) (1975) 1007–1016, https://doi.org/10.2514/3.60498.
[19] K. Holm-Jørgensen, S.R. Nielsen, A component mode synthesis algorithm for multibody dynamics of wind turbines, J. Sound Vib. 326 (3) (2009) 753–767, https://doi.org/10.1016/j.jsv.2009.05.007.
[20] D.-M. Tran, Reduced models of multi-stage cyclic structures using cyclic symmetry reduction and component mode synthesis, J. Sound Vib. 333 (21) (2014) 5443–5463, https://doi.org/10.1016/j.jsv.2014.06.004.
[21] J.-X. Yu, Y. Xia, W. Lin, X.-Q. Zhou, Element-by-element model updating of large-scale structures based on component mode synthesis method, J. Sound Vib. 362 (2016) 72–84, https://doi.org/10.1016/j.jsv.2015.10.019.
[22] Z. Ding, L. Li, Y. Hu, A free interface component mode synthesis method for viscoelastically damped systems, J. Sound Vib. 365 (2016) 199–215, https://doi.org/10.1016/j.jsv.2015.11.040.
[23] A. Girard, N. Roy, Structural Dynamics in Industry, vol. 7, John Wiley & Sons, 2010.
[24] M. Pascal, Dynamics analysis of a system of hinge-connected flexible bodies, Celest. Mech. 41 (1) (1987) 253–274, https://doi.org/10.1007/BF01238763.
[25] M.C. Bampton, R.R. Craig Jr., Coupling of substructures for dynamic analyses, AIAA J. 6 (7) (1968) 1313–1319, https://doi.org/10.2514/3.4741.
[26] R.R. Craig Jr., C.-J. Chang, Substructure Coupling for Dynamic Analysis and Testing, Tech. Rep. NASA-CR-2781, Texas University, Austin, TX, United States, 1977.
[27] K.H. Tantawi, D. Alazard, C. Cumer, Linear dynamic modeling of spacecraft with various flexible appendages, IFAC Proc. Vol. 41 (2) (2008) 11148–11153, https://doi.org/10.3182/20080706-5-KR-1001.01889.
[28] D. Alazard, J.A. Perez, T. Loquen, C. Cumer, Two-input two-output port model for mechanical systems, in: AIAA Science and Technology Forum and Exposition. Kissimmee, Florida, 2015, https://doi.org/10.2514/6.2015-1778.
[29] H.H.S. Murali, D. Alazard, L. Massotti, F. Ankersen, C. Toglia, Mechanical-attitude Controller Co-design of Large Flexible Space Structures, Springer, 2015, pp. 659–678, https://doi.org/10.1007/978-3-319-17518-8_38.
[30] J.A. Perez, D. Alazard, T. Loquen, C. Cumer, C. Pittet, Linear dynamic modeling of spacecraft with open-chain assembly of flexible bodies for acs/structure co-design, in: Advances in Aerospace Guidance, Navigation and Control: Selected Papers of the Third CEAS Specialist Conference on Guidance, Navigation and Control Held in Toulouse, Springer, 2015, pp. 639–658, https://doi.org/10.1007/978-3-319-17518-8_37.
[31] J.A. Perez, C. Pittet, D. Alazard, T. Loquen, C. Cumer, A flexible appendage model for use in integrated control/structure spacecraft design, IFAC-PapersOnLine 48 (9) (2015) 275–280, https://doi.org/10.1016/j.ifacol.2015.08.096.
[32] J.A. Perez, D. Alazard, T. Loquen, C. Pittet, C. Cumer, Flexible multibody system linear modeling for control using component modes synthesis and double-port approach, J. Dy. Syst. Meas. Control 138 (12) (2016), https://doi.org/10.1115/1.4034149 121004–121004–16.
[33] J. Chebbi, V. Dubanchet, J.A.P. Gonzalez, D. Alazard, Linear dynamics of flexible multibody systems, Multibody Syst. Dyn. 41 (1) (2017) 75–100, https://doi.org/10.1007/s11044-016-9559-y.
[34] R. Craig Jr., Coupling of substructures for dynamic analyses-an overview, in: 41st Structures, Structural Dynamics, and Materials Conference and Exhibit, 2000, p. 1573, https://doi.org/10.2514/6.2000-1573.
[35] The MSC Software Corporation, MSC Nastran 2012-Dynamic Analysis User's Guide.
[36] J.T. Young, Primer on Craig-bampton Cms Method: an Introductionto Boundary Node Function, Base Shake Analyses, Load Transformation Analyses, Modal Synthesis and Much More, Tech. Rep. NASA-CR-178510, NASA, 2000.
[37] R.D. Cook, D.S. Malkus, M.E. Plesha, R.J. Witt, Concepts and Applications of Finite Element Analysis, vol. 4, John Wiley & Sons, 2007.
[38] E. Reissner, On bending of elastic plates, Q. Appl. Math. 5 (1) (1947) 55–68.